Can NEXRAD and industry share the S-band? Exploring the impact of RF interference on the WSR-88D estimators

Bradley Isom[1,2] and Christopher Curtis[1,2]

[1]*Cooperative Institute for Mesoscale Meteorological Studies, The University of Oklahoma, Norman, OK*
[2]*NOAA/OAR National Severe Storms Laboratory, Norman, OK*

(Dated: 18 July 2014)

1. Abstract

Expanding use of wireless technology has prompted a dialogue concerning the reallocation of several bands within the RF spectrum. Included in the discussion is the 2.7 to 3.0 GHz band, where many meteorological and aircraft surveillance radars reside. Reducing the width of the allotted band or opening the band to additional transmitters will undoubtedly generate more instances of unwanted RF interference between radars. In an effort to quantify the potential impact, a simulation-based study was commissioned to explore the extent of the corruption through statistical means. RF interference can appear in three primary forms: pulsed, continuous wave, and noise-like. The scope of the study is limited to the effects of interference on Level-II base products, and performance is judged in terms of the NEXRAD Technical Requirements from the WSR-88D System Specification (ROC, 2008). Time series simulations are utilized to model the effects of interference on the estimation of meteorological variables. With the advent of the dual-polarization upgrade of the NEXRAD system, we consider all six of the meteorological variables that are sent as Level-II products: reflectivity (Z), Doppler velocity (v), spectrum width (σ_v), differential reflectivity ($Z_{\rm DR}$), differential phase ($\Phi_{\rm DP}$), and correlation coefficient ($\rho_{\rm hv}$). Previous technical reports such as ITU-R M.1464, ITU-R M.1849, NTIA TR-06-444, and NTIA TR-13-490 were reviewed to ensure that the study is consistent with established approaches for quantifying the impacts of interference on NEXRAD radars. A more detailed account of this study is available in a full technical report (Curtis and Isom, 2014).

In the next section, we summarize the types of interference that are examined in the study, explore the best way to apply the NEXRAD Technical Requirements to quantify the detrimental effects of interference, and define the scanning strategies that are used in the simulations. Subsequent sections explore the simulation methodology and results, and highlight some future considerations for interference on WSR-88D radars.

2. Introduction

2.1. Types of Interference

Three types of interference are considered in this study: pulsed, continuous wave (CW), and noise-like. The main focus is pulsed interference, especially from ASR radars and from other NEXRAD radars, but continuous-wave interference can be seen as an extreme type of pulsed interference when all of the samples at a particular range gate are affected. Noise-like interference also affects all of the samples at a particular range gate, but is incoherent and is treated separately. The different types of interference are explored in a set of illustrations presented in Figure 1.

The first example is of pulsed interference from a radar where the pulse repetition time (PRT) of the interfering radar is not an integer multiple of the PRT of the receiving radar. The pulse width of the interfering radar is also similar in width or shorter than the pulse width of the affected NEXRAD radar (1.57 μs for short pulse or 4.71 μs for long pulse), corresponding to interference from an ASR-8, ASR-9, or another NEXRAD radar. Figure 1(a) shows several range gates from this particular example. The columns in the figure represent the sampled returns from pulses transmitted by the radar. In the example shown, there are 9 pulses in a dwell. The number of pulses can vary from 3 in the batch mode for Volume Coverage Pattern (VCP) 12 to 278 in VCP 32. The radar is rotating as the pulses are transmitted, which causes them to be at slightly different azimuths and consequently different distances with respect to the center of the dwell. In this case, the center of the dwell is the azimuth of the fifth transmitted pulse and is labeled with a zero on the x-axis of Figure 1(a). The rows correspond to range gates with those at the top corresponding to range gates that are farther from the radar. Each row contains the samples that are used to estimate the meteorological variables for that particular range gate. The red dots represent samples directly affected by pulsed interference. This type of pulsed interference has the least effect on the estimation of meteorological variables since only one sample at a particular range gate is affected. We refer to this as single-hit interference because only a single sample at a particular range gate is corrupted.

The next example is similar to the first one, except the PRT from the interfering radars is an integer multiple of the PRT from the NEXRAD radar. When one PRT is an integer multiple of the other PRT, multiple samples can be affected by interference at a single range gate, which is illustrated in Figure 1(b). This leads to larger errors for the meteorological-variable estimates, but

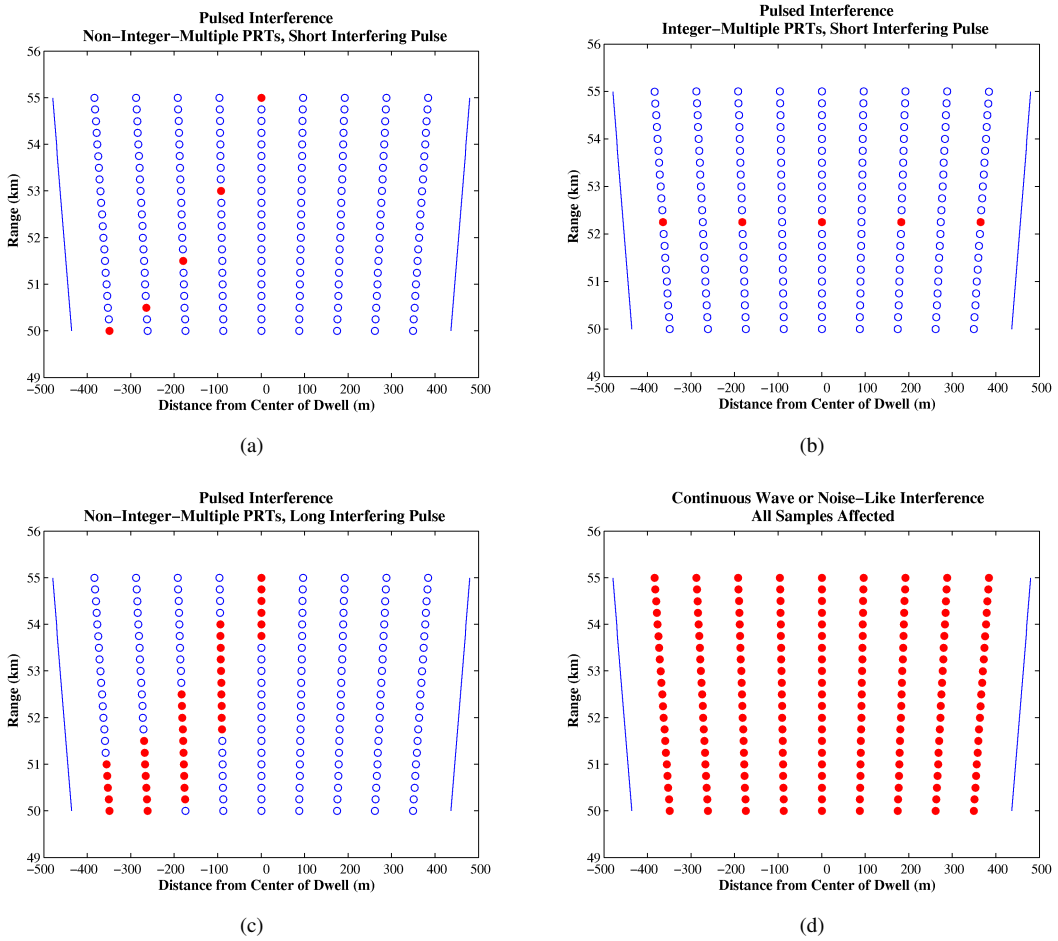

Figure 1: Illustrations representing several range gates, displaying the effects of different forms of pulsed and CW interference during a single radar dwell. The examples are (a) when the PRT of the interfering radar is not an integer multiple of the PRT of the affected NEXRAD radar and pulse widths are similar, (b) an integer multiple PRT, (c) longer interfering pulse with a non-integer multiple PRT, and (d) CW or noise-like interference. Rows are the samples corresponding to a single range gate. Red samples are corrupted by interference. In three of the examples, several range gates are affected by the pulsed or CW interference. One case illustrates a scenario when multiple pulses are corrupted within a single gate and dwell.

it affects fewer range gates. This situation should occur significantly less often than the first case since the chance of having two PRTs from independent radars be an exact integer multiple is less common than having non-integer-multiple PRTs.

The next example is also similar to the first one, except that the interfering radar is transmitting a longer pulse. The most common instance of this would be the long pulse utilized on the ASR-11. When the interfering radar transmits a longer pulse, it is more likely that a range gate will have more samples affected because of the larger number of samples that are corrupted by interference. In Figure 1(c), all of the range gates are affected by interference. In this example, range gates farther from the radar are affected with single-hit interference, and the range gates closer to the radar are affected with multiple-hit interference. It is expected that the multiple-hit interference will have a larger effect on the errors of meteorological-variable estimates than the single-hit case.

The last case shows the effects of either CW or noise-like interference. Even though these types of interference are different, they both affect all of the samples in every range gate because the interference is constantly being received. Figure 1(d) shows this case with all of the samples corrupted by interference. Continuous wave interference can be seen as the most extreme type of multiple-hit pulsed interference.

Through the rest of this study, we focus on the two extremes of single-hit and CW interference. The single-hit case affects the errors of meteorological-variable estimates the least with CW interference affecting the them the most, while other types of multiple-hit interference falling in-between. Noise-like interference is treated separately due to its different characteristics. Although noise-like and CW interference both affect all of the samples in a dwell, the CW interference is at a particular frequency and shows up as a peak in the Doppler spectrum. Noise-like interference increases the noise power at the receiver and affects all frequencies in the Doppler spectrum equally.

2.2. Applying NEXRAD Technical Requirements to Interference

The purpose of this study is to set interference-to-noise ratio (INR) thresholds based on simulations of meteorological variables (Level II products) using the NEXRAD Technical requirements. There are no particular requirements that specify the amount of interference allowed, so we derived specific requirements based on the existing ones. The basic precision (or standard deviation) requirements for each of the six meteorological variables are listed in Table 1. These are the requirements

Table 1: Precision requirements for the six meteorological variables from the WSR-88D System Specification (ROC, 2008).

Base Data Variable	**Standard Deviation**
Reflectivity	For a true spectrum width of 4 m s^{-1} the standard deviation in the estimate of the reflectivity will be less than or equal to 1 dB at SNR > 10 dB (including only the error due to meteorological signal fluctuations).
Mean Radial Velocity	For a true spectrum width of 4 m s^{-1} the standard deviation in the estimate of the mean radial velocity will be less than or equal to 1.0 m s^{-1} including quantization errors, for SNR greater than 8 dB.
Spectrum Width	For a true spectrum width of 4 m s^{-1} the standard deviation in the estimate of the spectrum width will be less than or equal to 1.0 m s^{-1} including quantization errors, for SNR greater than 10 dB.
Differential Reflectivity[1]	For a spectrum width of 2 m s^{-1}, correlation coefficient $\geq$ 0.99, and dwell time of 50 ms, the standard deviation in the estimate of the differential reflectivity will be less than 0.3 dB for $SNR \geq$ 20 dB.
Correlation Coefficient	For a true spectrum width of 2 m s^{-1}, correlation coefficient $\geq$ 0.99, and dwell time of 50 ms, the standard deviation in the estimate of the correlation coefficient will be less than 0.006 for $SNR \geq$ 20 dB.
Differential Phase	For a true spectrum width of 2 m s^{-1}, correlation coefficient $\geq$ 0.99, and dwell time of 50 ms, the standard deviation in the estimate of the differential will be less than 2.5° for $SNR \geq$ 20 dB.

that specify the standard deviation of the meteorological-variable estimators under a certain set of conditions. For example, the reflectivity standard deviation requirement is 1 dB at an SNR of 10 dB and a true spectrum width of 4 m s^{-1}. The other requirements are similar in that the requirement is set for a specific set of conditions, including the true correlation coefficient for the polarimetric variables. Unfortunately, it is difficult to directly apply these requirements to interference. We are concerned about the effects of interference at all SNR values, not just the particular ones listed in the requirements. For example, the polarimetric-variable requirements are set at an SNR of 20 dB, but interference could cause significant problems at lower SNR values. Also, for VCP 12, the requirements in Table 1 are barely met; this could lead to a determination where no interference may be allowed at all. In addition to the standard deviation requirements, there is also a bias requirement for reflectivity estimates that mandates absolute calibration within 1 dB; we are focusing on the precision requirements that apply

[1]The differential reflectivity requirement is being updated to 0.4 dB by the ROC.

to the estimation (rather than calibration) of the meteorological variables. Our decision is to use the requirements as a starting point to find a reasonable way to look at the effects of interference for a wide range of SNR values.

In addition to requirements listed in Table 1, there are also requirements related to ground clutter filtering. In some ways, the effects of interference are similar to the effects of ground clutter: a non-weather signal is degrading the quality of meteorological variable estimates. The main difference lies in the fact that there are ground clutter filters in the signal processor that help to mitigate the effects on the estimates, while there is no such filter for interference signals. The requirements are set assuming that the user is gaining something from the ground clutter filtering, which results in a relaxation of the normal requirements. Currently, there are no specific filters used to mitigate the effects of electromagnetic interference on NEXRAD radars. The radial-by-radial noise estimator that is discussed in Section 4 can remove some of the effects of noise-like interference, but the interference still affects the sensitivity of the radar. Even if there were filters designed specifically to remove interference, they do not necessarily work the same way as ground clutter filters. For example, a pulsed interference filter could remove very strong interference spikes but leave weaker (more difficult to detect) spikes that still affect the meteorological variable estimates. Another difference is the fact that ground clutter is always present to a certain extent, but siting and spectrum allocation can be used to mitigate interference. Because of these differences, we adopted the same types of requirements that are used for ground clutter filtering, but with somewhat more stringent limits for interference.

The ground clutter requirements are written in terms of "maximum allowable bias in reflectivity estimates due to the clutter suppression device" (ROC, 2008). We refer to this as the delta bias (ΔBias) since it is in addition to the inherent bias of the estimator. For example, the most stringent clutter requirement for reflectivity is a maximum allowable bias of 1 dB. This means that the bias of the estimator with clutter present must be within 1 dB of the inherent bias of the estimator. This requirement structure also works well for interference since interference is an external source of estimation bias. The key decision then becomes setting limits on the ΔBias for each of the meteorological variables. Historically, the ΔBias limits for interference have been set based on the standard deviation limits from the requirements listed in Table 1. This results in a ΔBias limit of 1 dB for reflectivity, and 1 m s^{-1} for both velocity and spectrum width at all SNRs. The ΔBias for reflectivity is measured in dB rather than dBZ because it is the ratio of two linear values (in logarithmic units). These values were used in NTIA Report TR-06-444 (2006) for reflectivity and spectrum width. We also found the same limits suggested by Dale Sirmans in internal documents that were written during his long career at the Radar Operations Center. These limits are more stringent than the ground clutter limits that are stated in the requirements document, but they are directly related to the standard deviation requirements (listed in Table 1).

In the same way that ΔBias measures the deviation from the inherent bias of the estimator, we can also look at deviation from the inherent standard deviation of the estimator. For ground clutter, this is described in the requirements as "bias and standard deviation contributions by the clutter suppression device" (ROC, 2008). For interference, we are capturing bias and standard deviation contributed in addition to the inherent bias and standard deviation of the estimators. The delta standard deviation (ΔSD) is similar to the ΔBias but can be used in particular situations where the ΔBias is not sensitive to interference. We will see examples of this for the radial velocity pulsed interference simulation in Section 3. Just as with the ΔBias, we need to determine limits for ΔSD that are reasonable and are derived from the system requirements. Historically, the same limits are used for ΔSD that are used for ΔBias. This gives a consistent way to quantify the effects of interference on both the bias and standard deviation of the meteorological-variable estimators.

Limits were given for reflectivity, velocity, and spectrum width, but not for the polarimetric-variable estimators. This is examined in more detail in Section 3, but the main reason is due to the very large biases and standard deviations of the polarimetric variables at low SNR values. The inherent biases and standard deviations at low SNR are many times larger than the standard deviation requirements stated in Table 1. In contrast, the inherent biases and standard deviations for reflectivity, velocity, and spectrum width at low SNR are only a few times larger than the standard deviation requirements. In general, the polarimetric-variable estimators are much more sensitive to noise, which makes it very difficult and somewhat meaningless to measure changes in ΔBias or ΔSD at low SNR. We will focus on reflectivity, velocity, and spectrum width when analyzing the simulations. Because all of these variables are only computed using the horizontal polarization channel, the horizontal interference power should be the main focus when utilizing the INR thresholds.

The 1-dB and 1-m s^{-1} limits are reasonable for non-meteorological interference that comes from an external source, but is not necessarily present at all sites like ground clutter. For completeness, we also address two other possible ΔBias and ΔSD limits in the main report (Curtis and Isom, 2014), but omit the results for this discussion. In the report, we include ΔBias limits of 2 dB and 0.5 dB for reflectivity and ΔBias and ΔSD limits of 2 m s^{-1} and 0.5 m s^{-1} for velocity and spectrum width. These additional values provide a way to examine the effects of varying the ΔBias and ΔSD limits on the INR thresholds.

2.3. Volume Coverage Patterns

Now that we have looked at the different types of interference and the derived requirements that are used to determine the INR thresholds, we can identify the scanning strategies that are most sensitive to interference. By focusing on the most sensitive strategies, we can capture the effects of interference without looking at every possible scanning strategy or combination of acquisition parameters. NEXRAD operational VCPs fall into two major categories: precipitation and clear air. Clear-air VCPs are used when there is little or no precipitation, and sometimes in cases of light snow: VCP 31 and VCP 32. Precipitation VCPs are used when significant precipitation is present: VCP 11, VCP 12, VCP 21, VCP 121, VCP 211, VCP 212, and VCP 221.

The VCPs are collections of sweeps (360° revolutions of the antenna) at different (constant) elevation angles (also called cuts). At low elevation angles, there can be more than one sweep. For example, a split sweep (also referred to as a "split cut") is made up of two sweeps at the same elevation angle with a different PRT for each sweep. The first sweep, or surveillance sweep, uses a long PRT, while the second sweep, or Doppler sweep, uses a shorter PRT.

Another type of sweep that uses two PRTs is the batch sweep. The batch sweep alternates sets of long and short PRTs during a single sweep. The two sets of pulses from both PRTs form a single dwell for processing. As with the split sweep, the long PRT pulses are referred to as the "surveillance pulse" and short PRT pulses are the "Doppler pulse". The last type of sweep, continuous Doppler, is used at high elevation angles and consists of a single PRT.

At each elevation angle in a VCP, the meteorological-variable estimates are censored so the estimates with poor quality due to noise contamination are eliminated from the display. The VCP has a set of SNR thresholds at each elevation to determine which estimates are visible. For example, the default SNR threshold for the surveillance sweep that is part of the 0.5° split sweep from VCP 12 is 2.0 dB. For the Doppler sweep that is also part of the same split sweep, the default SNR threshold is 3.5 dB. Although the default values can be changed by the forecasters, we use the default values in the simulations because they are seldom modified in practice. These SNR thresholds represent the lower end of SNR values where estimates are displayed and are where the effects of interference are most pronounced.

For this study, we identified one clear-air and one precipitation VCP that are especially susceptible to interference. Clear-air VCP 31 has the lowest default SNR threshold at 0 dB. This is the same VCP that was used in the meteorological radar testing section of ITU-R M.1464 (1998). The low default SNR threshold makes it more sensitive to interference than the other clear-air VCP (VCP 32). We chose precipitation VCP 12 because it has the fastest update rate (fewer pulses per dwell), is used the most often for the convective events associated with severe weather, and the standard deviations of the estimators barely meet requirements. Both of the VCPs are described in Tables 2 and 3, respectively, and particular elevation sweeps are chosen for later exploration through simulations. The split sweep surveillance and Doppler scans are abbreviated with SS and SD, and

Table 2: Scan parameters for VCP 31 for the surveillance and Doppler sweeps at the lowest elevation angles.

Scan Type	Elevation	PRT (ms)	$\mathbf{v_a}$ m s^{-1}	Pulses	$\mathbf{SNR_{th}}$ (dB)	Output
SS	0.5-2.5°	3.12	8.43	63	0.0	Z,Z_{DR},Φ_{DP},ρ_{hv}
SD	0.5-2.5°	2.25	11.7	87	0.0	v,σ_v

Table 3: Scan parameters for VCP 12 for the lowest elevation split sweep (0.5°) and the lowest elevation batch sweep (1.8°).

Scan Type	Elevation	PRT (ms)	$\mathbf{v_a}$ m s^{-1}	Pulses	$\mathbf{SNR_{th}}$ (dB)	Output
SS	0.5°	3.12	8.44	15	2.0	Z,Z_{DR},Φ_{DP},ρ_{hv}
SD	0.5°	0.986	26.7	40	3.5	v,σ_v
BS	1.8°	3.12	8.44	3	3.5	Z,Z_{DR},Φ_{DP},ρ_{hv}
BD	1.8°	0.986	26.7	29	3.5	Z,v,σ_v,Z_{DR},Φ_{DP},ρ_{hv}

the batch sweep scans are similarly represented by BS and BD. Higher elevation scans are not considered in this study.

An additional attribute of VCP 31 that needs to be considered is that it utilizes a 4.71-μs transmitted pulse (long pulse) instead of the 1.57-μs transmitted pulse (short pulse) used for the other VCPs. This leads to a lower noise power when compared to the VCPs that use the short pulse after the matched filter is applied. The simulations that were implemented to study the effects of interference set the SNR based on the post-matched-filter noise power. This should be taken into account when employing the INR thresholds because the same level of interference will result in a different INR threshold (INR_{th}) for different pulse lengths. The noise power depends on the matched-filter bandwidth, which is typically tied to the length of the pulse (long or short).

The rest of the paper is organized as follows. Section 3 describes the methods used to simulate time series data and how the INR thresholds are derived from the simulations. Section 4 discusses the effects of noise-like interference on the system. Section 5 explores some possible future changes to the NEXRAD system that could influence the results. Finally, Section 6 summarizes the effects of interference and our approach to quantifying them.

3. Pulsed and Continuous Wave Interference

In this section, the effects of pulsed and CW interference are studied using time series simulations. First, the time series simulations are described including models for both types of interference. The polarimetric variables are then discussed focusing on why they are not used to determine INR thresholds. The next two sections summarize the results for pulsed and CW interference, respectively, and provide the INR thresholds that are based on the simulations.

3.1. Simulation Methodology and Theory

The weather simulator developed for this study utilizes a technique developed by Zrnić (1975), but expanded to include polarimetric signals (Galati and Pavan, 1995). The weather simulator produces dual-polarization time series data based on the true values of all six meteorological variables (Z, v, σ_v, $Z_{\rm DR}$, $\Phi_{\rm DP}$, $\rho_{\rm hv}$), and interference models are used to generate corrupting signals, which are then added to the simulated weather. The algorithms used to process the data in the simulations are the same algorithms implemented on the NEXRAD radars. Because the interference signals are relatively simple to model, simulations can accurately capture the effects of interference over a wide range of conditions. A block diagram of the weather-interference simulator is presented in Figure 2, which will be referenced in the subsequent discussion.

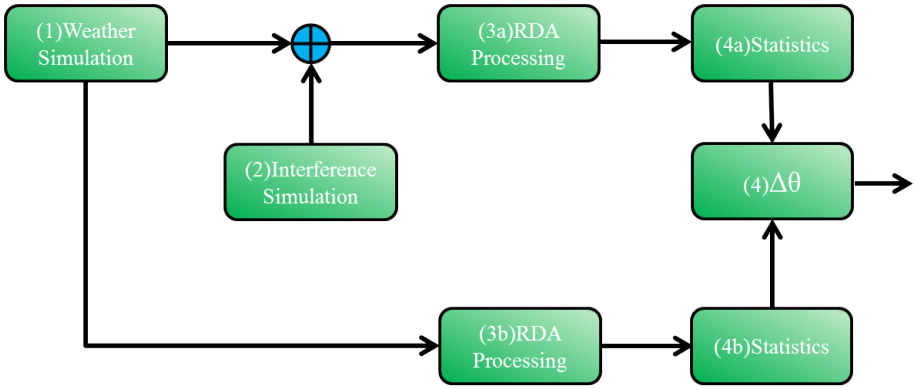

Figure 2: A block diagram of the weather-interference simulator. Two paths for the simulated weather data are maintained to allow for comparisons and direct calculations of the statistical impact to the meteorological variables.

Block 1, the Weather Simulation, takes the true values of the meteorological variables (Z, v, σ_v, $Z_{\rm DR}$, $\Phi_{\rm DP}$, $\rho_{\rm hv}$) as input as well as the number of samples (M), the noise power (N), and signal-to-noise ratio (SNR). For the simulations and without loss of generality, the horizontal and vertical channel noise powers are assumed to be the same. Two complex time series channels are produced at the output representing the horizontal and vertical channel data. For this study, 100,000 realizations are simulated to achieve accurate statistical results.

Block 2 generates the interference data for both pulsed and continuous wave interference. The noise-like interference case is not considered in the simulations and is addressed separately in Section 4. Pulsed interference is modeled as a single hit with random phase $\phi_{\rm p}$. The interference powers, $I_{\rm h}$ and $I_{\rm v}$, are used in the definitions of the INR ($INR = I_{\rm h}/N$) and the differential interference ratio ($I_{\rm DR} = I_{\rm h}/I_{\rm v}$). Note that the INR value is taken as the direct ratio between the interference and noise powers, and is based on the horizontal channel. That is, INR is equal to one (or zero dB) when the interference from the horizontal channel is equal to the noise. $I_{\rm DR}$ is defined as the ratio between the horizontal and vertical channel interference powers; thus, the vertical interference power is determined by the horizontal interference power and the $I_{\rm DR}$.

To accurately represent single-hit pulsed interference, the temporal location of the interference pulse within the dwell is selected at random and all other samples in the dwell are set to zero. The pulsed-interference time series signals at a particular range gate are defined in Equation 3.1:

$$\begin{aligned} V_{\rm h}(m) &= \begin{cases} \sqrt{I_{\rm h}} exp\left[j\phi_{\rm p}\right], & \text{if } m = k \\ 0, & \text{otherwise} \end{cases}, \\ V_{\rm v}(m) &= \begin{cases} \sqrt{I_{\rm v}} exp\left[j(\phi_{\rm p} + \alpha)\right], & \text{if } m = k \\ 0, & \text{otherwise} \end{cases} \end{aligned} \tag{3.1}$$

where m is the sample index from 1 to M, $j = \sqrt{-1}$, $\phi_{\rm p}$ is a uniform random variable between 0 and $2n$, and k is an integer-valued random variable between 1 and M. The additional α in the vertical channel captures the phase difference between the channels based on the transmitted polarization.

CW interference is modeled as a single tone (frequency) that is within the passband of the radar receiving the interference. The interfering signal appears at an apparent Doppler velocity $v_{\rm CW}$. The initial phase of the tone, $\phi_{\rm CW}$, is a uniform random variable between 0 and $2n$, and the interference powers, $I_{\rm h}$ and $I_{\rm v}$, are again defined by the INR and $I_{\rm DR}$ values.

A mathematical expression for the CW-interference time series signals is given in Equation 3.2:

$$\begin{aligned} V_{\mathrm{h}}(m) &= \sqrt{I_{\mathrm{h}}} exp\left[-j(4\pi v_{\mathrm{CW}} m T_{\mathrm{s}}/\lambda + \phi_{\mathrm{CW}}\right], \\ V_{\mathrm{v}}(m) &= \sqrt{I_{\mathrm{v}}} exp\left[-j(4\pi v_{\mathrm{CW}} m T_{\mathrm{s}}/\lambda + \phi_{\mathrm{CW}} + \alpha\right] \end{aligned} \tag{3.2}$$

where T_{s} is the PRT, m is the sample index from 1 to M, and λ is the transmitter/radar wavelength. The α value captures the effect of the transmitted polarization of the interference. In both the pulsed and CW interference cases, horizontal and vertical complex time series data are produced.

One branch of the simulator shown in Figure 2 preserves the weather time series, while the other sums the interference signal with the weather. Preserving both the original and corrupted signals allows for direct statistical comparisons to be made. The subsequent stage of the simulator (Block 3) calculates the traditional weather radar variables (Z, v, σ_v, Z_{DR}, Φ_{DP}, ρ_{hv}) for the corrupted and uncorrupted signal paths using processing based on the Radar Data Acquisition (RDA) unit of the NEXRAD receiver subsystem. In Block 4, the bias and standard deviation are computed for each of the meteorological variables. Block 4(b) computes the inherent bias and standard deviation of the estimators, and Block 4(a) includes the additional bias and standard deviation introduced by the interference. Then, in Block 5, the ΔBias and ΔSD are calculated for each meteorological variable, which is denoted by the $\Delta\theta$ symbol in the diagram. The difference calculation allows for the extent of the impact of the interference on the meteorological variables to be ascertained while accounting for the inherent bias and standard deviation of the estimators themselves. Statistics are then examined and collated to create meaningful illustrations and to find INR_{th} values.

3.2. Polarimetric Variables

As mentioned in the previous section, the polarimetric variables are not used to determine the INR thresholds. In this section, we show an example using the differential reflectivity (Z_{DR}) to better illustrate some of the issues with utilizing the polarimetric variables for this purpose. The other two polarimetric variables, differential phase and correlation coefficient, behave very similarly to Z_{DR} at low SNR values and do not add significantly to the discussion.

Figure 3 shows the bias and standard deviation of Z_{DR} over a wide range of INR values when pulsed interference is added to the weather signal. Shown in the figure is the total bias and standard deviation from both signals, and not the ΔBias and ΔSD that will be used in subsequent sections. Figure 3(a) and Figure 3(c) show the bias and standard deviation with a true Z_{DR} of 0.2 dB and an I_{DR} of 0 dB, while Figure 3(b) and Figure 3(d) utilize the same statistical parameters, except the true Z_{DR} is 4.5 dB. The SNR for the weather signal is kept constant at 3.5 dB based on the SNR threshold for the Doppler part for the batch sweep (BD) in VCP 12. The true Z_{DR} of 0.2 dB would most often occur in light rain, and the true Z_{DR} of 4.5 dB is a more extreme case that could occur in certain types of hail.

There are two main issues with using the polarimetric variables for determining INR thresholds. The first is the variability in the bias and standard deviation at low SNR values. This variability is apparent in all four plots in Figure 3. This variability would lead to extremely low INR thresholds that were not due to interference, but instead to spikes in the bias and standard deviation values. One solution to the variability issue would be to significantly increase the number of realizations in the simulations to attempt to only capture the effects of interference. Running enough simulations is probably not practical in this case because of the other issue with using the polarimetric variables: the standard deviations from the requirements are very small compared to the biases and standard deviations shown in Figure 3, making the measurement meaningless. For example, the standard deviation of the weather signal alone in Figure 3(c) is around 6 dB (and even larger for Figure 3(d)). The standard deviation requirement of 0.3 dB is also shown in these two plots. The standard deviation at low SNR values is so large compared to the ΔSD limit of 0.3 dB that it makes the ΔSD irrelevant.

The difference between the polarimetric variables and the meteorological variables (Z, v, σ_v) is this large discrepancy between the standard deviation requirements and the bias and standard deviations at low SNR. The requirements for the polarimetric variables are set at a higher SNR value (20 dB) than the 8 or 10 dB for the other variables. Additionally, the polarimetric variables are just more sensitive to noise which makes it extremely difficult to measure the effects of interference at low SNR values. For these reasons, the INR thresholds are determined based on reflectivity, velocity and spectrum width.

3.3. Pulsed Interference

Pulsed interference occurs when a surveillance radar interferes with another surveillance radar. This study specifically focuses on the interference from ASR-8, 9, and 11 radars on NEXRAD radars, as well as the interference from NEXRAD radars on other NEXRAD radars. As described in the simulation methodology, pulsed interference is modeled as a single hit at one range gate. This is the smallest effect that pulsed interference can have on a range gate, but this is a reasonable place to start since pulsed interference only affects a relatively small fraction of range gates in a sweep. This section examines the effects of pulsed interference on reflectivity, velocity, and spectrum width, and provides INR thresholds based on derived requirements. The results will be summarized to show the minimum INR thresholds for the three scan types: VCP 12 batch

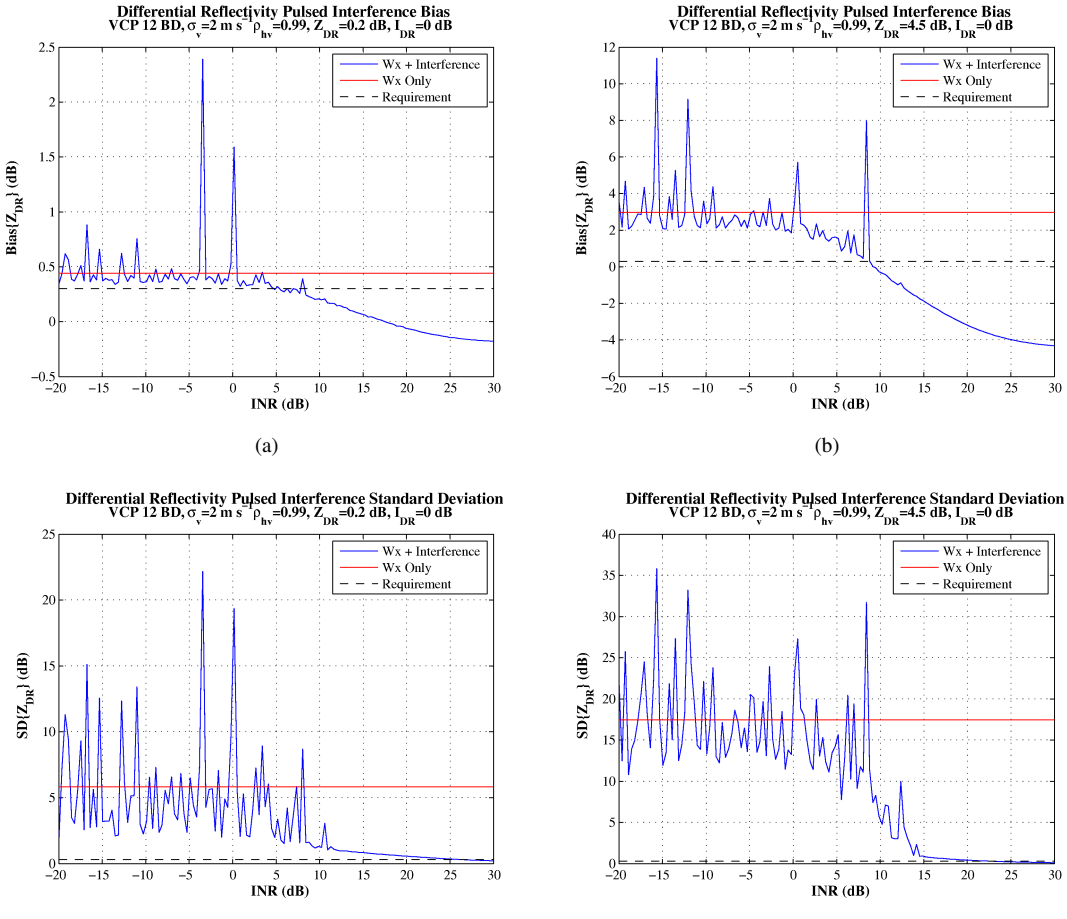

Figure 3: The Z_{DR} bias and standard deviation as a function of INR with a true Z_{DR} of 0.2 dB, (a) and (c), and 4.5 dB, (b) and (d). The solid red horizontal line represents the mean inherent bias or standard deviation without interference, and the dashed horizontal line represents the 0.3 dB threshold based on the dual-polarization requirements in Table 1.

sweep, VCP 12 split sweep, and VCP 31 split sweep. Finally, the fraction of range gates corrupted by pulsed interference for different interfering radars is addressed.

3.3.1. Reflectivity

Reflectivity is one of the most utilized and intuitive meteorological variables. It measures the backscattering cross section of the hydrometeors in a resolution volume and is derived from the received signal power. Reflectivity is used in many downstream algorithms such as rainfall estimation, which aid in the delivery of flood watches and warnings. In this section, we examine the effects of pulsed interference on reflectivity estimates by looking at ΔBias and ΔSD.

To better understand the method for determining INR thresholds, a single case is examined in detail. The reflectivity ΔBias for the batch Doppler case from VCP 12 is shown in Figure 4. The SNR of the weather is set to the default SNR

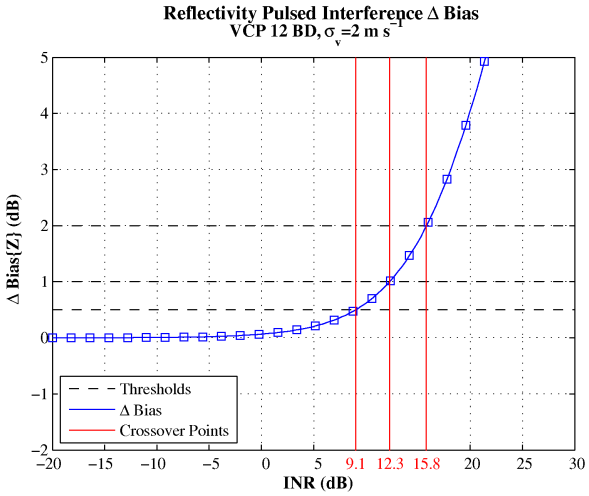

Figure 4: An example of the reflectivity ΔBias as a function of INR for pulsed interference. The dashed black lines represent the three limits under consideration, i.e., 0.5, 1, and 2 dB. The vertical red lines indicate the points at which the ΔBias crosses the limits (determining the INR thresholds) with the exact values indicated in red on the abscissa.

threshold for this case, which is 3.5 dB. This reflects the low SNR values near the SNR threshold where the interference should have the most effect. We decided to use a true spectrum width of 2 m s^{-1} for all of the simulations presented in this paper rather than looking at the worst case spectrum width. The value of 2 m s^{-1} is the median for most weather events (Fang et al., 2004) and is a reasonable choice when focusing on a single value. Other spectrum widths are considered in the full report, along with the worst case values of the INR thresholds.

At low INR values, the ΔBias is zero because the interference is not influencing the ΔBias value. In general, the reflectivity estimator is unbiased so the ΔBias will directly measure the bias induced by the interference. As the INR increases, the ΔBias also increases as the pulsed interference starts to corrupt the weather signal. We included all three of the ΔBias limits (the dashed horizontal lines at 0.5, 1, and 2 dB) in this example to show how the limits affect the $INR_{\rm th}$. In this case, the curve crosses the first threshold of 0.5 dB at 9.1-dB INR. This crossing point gives the $INR_{\rm th}$ for the 0.5-dB limit because this is the INR value where the ΔBias equals the limit. The $INR_{\rm th}$ for the 1-dB limit is 12.3 dB and for the 2-dB limit is 15.8 dB. Based on this plot, the $INR_{\rm th}$ for this case is set to 12.3 dB since this is the threshold for the 1-dB limit. In subsequent figures, only the 1-dB limit will be included.

Figure 5(a) shows the reflectivity ΔBias for all four cases where reflectivity is calculated. Note that the weather signal SNR depends on the default SNR threshold for each of the cases: 3.5 dB for VCP 12 BS, 2 dB for VCP 12 SS, 3.5 dB for VCP 12 BD, and 0 dB for VCP 31 SS. As shown in the previous figure, the ΔBias increases with INR. The $INR_{\rm th}$ depends on the number of samples used for the estimate since the fraction of pulses affected is larger when the number of samples is smaller.

The VCP 12 BS case uses only three samples, and results in the lowest INR threshold. As the number of samples increases, the INR threshold increases, indicating a greater tolerance to interference. Although VCP 31 SS utilizes more samples (63) than VCP 12 BD (29), the curves are similar because of the lower default SNR threshold in VCP 31 (0 dB vs. 3.5 dB for VCP 12). In general, the $INR_{\rm th}$ increases with increasing number of samples and increasing weather signal SNR.

Figure 5(b) shows the ΔSD for the same four cases as in Figure 5(a). The curves decrease with increasing INR instead of increasing as in Figure 5(a). The standard deviation of the combined weather and interference signal decreases because the interference signal has a fixed power that dominates as the INR increases. This results in a negative ΔSD value because the standard deviation of the combined signal is less than the standard deviation of the weather signal alone. Although this could be seen as an 'improvement' in the performance, it is actually a result of the interference signal dominating. For reflectivity, the

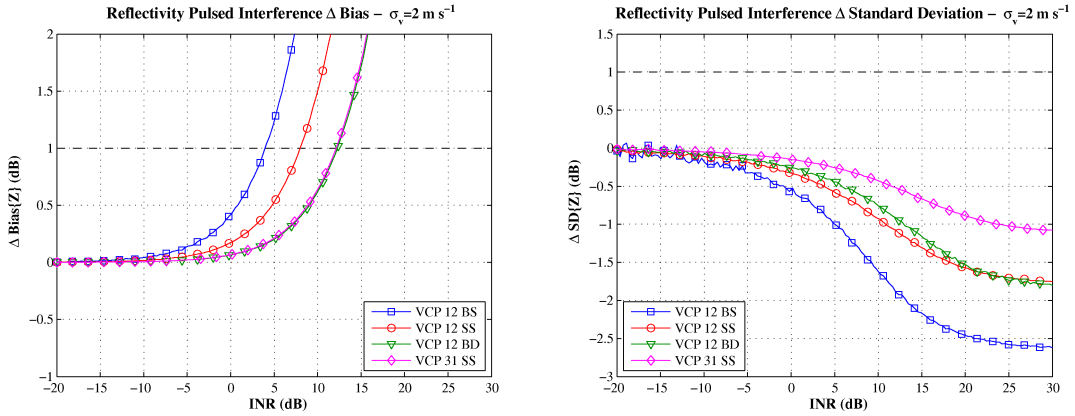

(a) (b)

Figure 5: Reflectivity (a)ΔBias and (b)ΔSD as a function of INR for pulsed interference depicting four cases associated with VCP 12 and 31. The 1-dB limit is denoted by the dashed horizontal line. An increase in tolerance is visible as the sample size increases for the ΔBias plot, while the ΔSD curves never cross the limit, and thus no $INR_{\rm th}$ is assigned in any of the ΔSD cases.

ΔBias will be used to set the INR thresholds, and no INR thresholds for ΔSD will be assigned for any of the cases because the threshold is not crossed.

The INR thresholds for reflectivity ΔBias are presented in Table 4 at the end of this section, along with results for radial velocity and spectrum width. These are the thresholds for a spectrum width of 2 m s^{-1}, and ΔBias and ΔSD limits of 1 dB. The 1-dB limit for ΔSD was not exceeded for any of the test cases and is omitted from the table. The table is organized in a hierarchical manner with VCP as the primary designator, followed by scan type. Dark gray cells indicate that the scan is not used to calculate reflectivity; all four cases where reflectivity is calculated are shown in the tables. The lowest $INR_{\rm th}$ appears in the VCP 12 BS case with a value of 3.9 dB.

3.3.2. Radial Velocity

The radial velocity estimator measures the mean velocity of the hydrometeors within the resolution volume, in the direction of the radar radial. Detection of wind shear and mesocyclone vortices are important uses of the radial velocity estimator, and biases in the measurement of velocity can impact the ability to identify areas of potential risk for life and property. Radial velocity is not a biased estimator, meaning that any bias observed during the interference study is due to the influence of the corrupting signal. As with reflectivity, the effects of pulsed interference on ΔBias andΔSD are examined.

The radial velocity ΔBias is not especially illuminating because pulsed interference does not induce a bias in the velocity estimator. Figure 6(a) shows the ΔBias for the three cases where velocity is estimated. As with the reflectivity simulations, the weather signal SNR is set based on the default SNR thresholds: 3.5 dB for VCP 12 BD and VCP 12 SD, and 0 dB for VCP 31 SD. Because pulsed interference is an impulse in the time domain, it appears flat in the spectral domain. This means that the effects of increasing INR are similar to the effects of increased noise. The bias is zero, but the standard deviation of the estimator increases. Figure 6(b) illustrates the effects of pulsed interference on the velocity ΔSD. As expected, the ΔSD increases with increasing INR. Although it is not shown in the figure, the ΔSD curves approach asymptotic values at very large INRs because the standard deviation saturates when the spectrum becomes completely flat. The asymptotic values depend on the PRT since the maximum unambiguous velocity determines the width of the spectrum. We will also see the effects of this flat spectrum when we examine the spectrum width estimator. As with the reflectivity, the ΔSD $INR_{\rm th}$ increases with increasing number of samples. The VCP 12 BD case (29 samples) has the lowest $INR_{\rm th}$, and the VCP 31 SD case (87 samples) has the largest $INR_{\rm th}$.

The values of the INR thresholds determined from the ΔSD curves are captured in Table 4. No ΔBias values are presented in the table. The INR thresholds are higher for velocity than for reflectivity, which indicates that the reflectivity estimator is more sensitive to pulsed interference.

3.3.3. Spectrum Width

Spectrum width provides valuable information about turbulence and velocity dispersion within the resolution volume. In order to match the processing on the NEXRAD radars, the same hybrid spectrum width estimator was utilized in the simulations that is currently implemented on the NEXRAD system. This estimator returns either the R_1/R_3, R_1/R_2, or R_0/R_1 estimate depending on a preliminary spectrum width calculation. The algorithm was implemented as described in the National Center

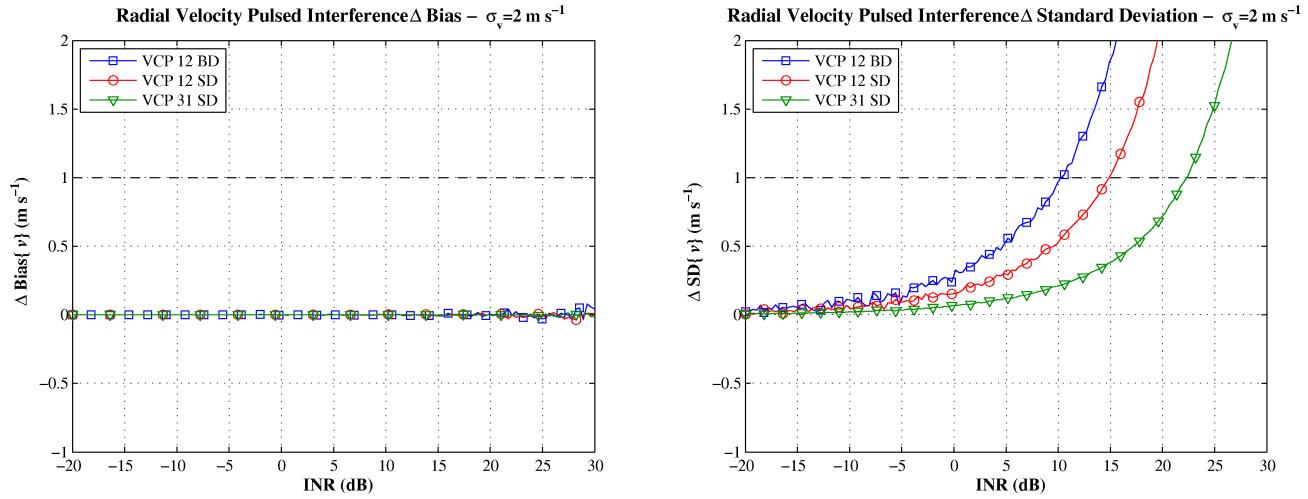

(a) (b)

Figure 6: Radial velocity (a)ΔBias and (b)ΔSD as a function of INR for pulsed interference depicting three cases from VCP 12 and 31. The 1-m s^{-1} limit is denoted by the dashed horizontal line. No dependence on the true v is observed for pulsed interference.

for Atmospheric Research (NCAR) Annual Report (2009). The spectrum width values are then clipped at $v_a/\sqrt{3}$, where v_a is the maximum unambiguous velocity.

The spectrum width ΔBias is plotted in Figure 7(a) for the same three cases that were used for velocity. The results are

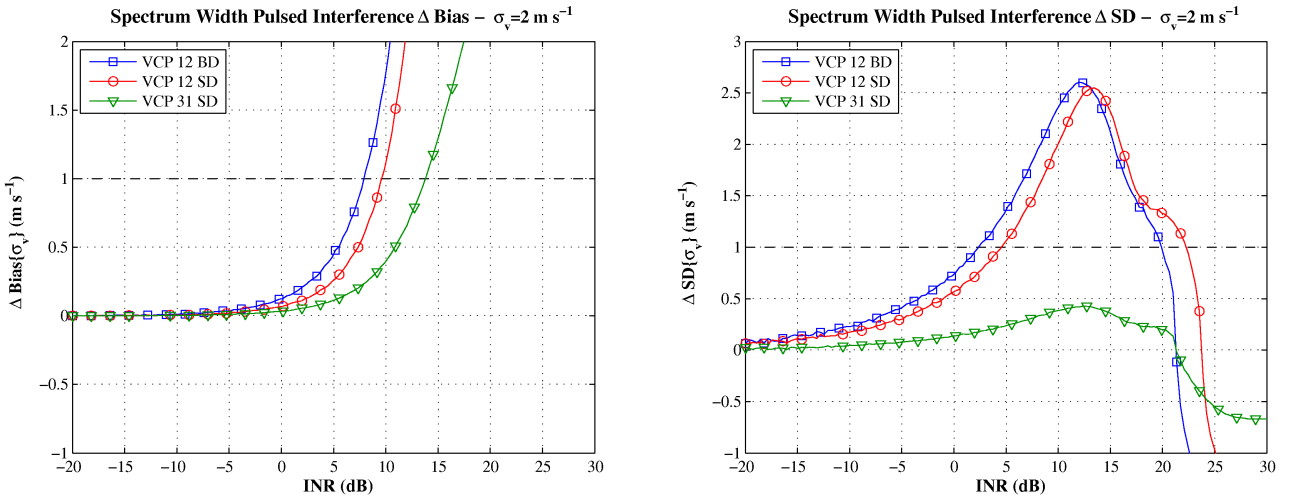

(a) (b)

Figure 7: Spectrum width (a)ΔBias and (b)ΔSD as a function of INR for pulsed interference depicting the same three cases used for velocity. The 1-m s^{-1} limit is denoted by the dashed horizontal line. As with the radial velocity, no dependence on v is observed for pulsed interference.

similar to the ΔSD velocity plots, which makes sense since spectrum width is related to the standard deviation of the velocity. As with the ΔSD velocity plots, the ΔBias curves approach asymptotic values at high INR values because of saturation, and the asymptotic values are related to the PRT (and corresponding maximum v_a). The same relationship between the INR thresholds and the number of samples is seen with larger INR thresholds corresponding to larger numbers of samples.

For the spectrum width ΔSD, the results are more complicated. Figure 7(b) shows that the ΔSD curves start to increase with INR, but then they decrease after a certain point, eventually obtaining negative values. Negative values indicate that the standard deviation of the sum of the weather and interference signals over this range is less than the standard deviation of the weather signal alone. This occurs because the spectrum width of the interference signal is large and saturates at the clipped value when the INR is high. When the clipped value dominates, the variance approaches zero leading to the negative ΔSD values. The curve for the VCP 31 SD case never crosses the 1-m s^{-1} limit at the displayed INR values. Therefore, there is no INR_{th} shown in Table 4 for the VCP 31 SD case (this is denoted with a '-' symbol). The other two curves also decrease after a certain point, but only after they have crossed the 1-m s^{-1} limit. As with the ΔBias, the INR_{th} increases with increasing numbers of samples.

The ΔSD provides the minimum spectrum width INR thresholds in the cases where it is defined, and the ΔBias provides the minimum threshold in the VCP 31 SD case. The spectrum width estimator is the most sensitive to interference for the two VCP 12 cases, but reflectivity is the driver for VCP 31 case. The sensitivity of the spectrum width estimator to interference is consistent with the findings in ITU-R M.1464 (1998). The INR thresholds are captured in Table 4 at the end of this section, which combines the results for all three meteorological variables.

3.3.4. Results Summary

Table 4 shows the INR thresholds for reflectivity, velocity, and spectrum width for pulsed interference. The minimum threshold for each case is found in the bottom row of the table and is shown in bold. For pulsed interference, spectrum width is the driver, except in the VCP 31 case where reflectivity provides the minimum threshold. The lowest overall INR_{th} for pulsed interference is 2.4 dB, and this number could be used to inform siting and spectrum allocation decisions. However, the VCP 12 batch sweep and the VCP 12 split sweep are utilized at different elevation angles. The VCP 12 batch sweep is collected at 1.8° and may be affected differently by pulsed interference than the VCP 12 split sweep at 0.5°. If the main concern is with interference at the lowest elevation angles of typical scanning strategies, an INR_{th} value of 4.5 dB may be used instead.

Table 4: INR Thresholds - Pulsed Interference - Summary - σ_v= 2 m s^{-1}

	VCP 12				VCP 31	
Scan	**BS**	**BD**	**SS**	**SD**	**SS**	**SD**
$\boldsymbol{INR_{\mathrm{th}}}$ **(dB) Ref ΔBias**	3.9	12.3	8.0		12.1	
$\boldsymbol{INR_{\mathrm{th}}}$ **(dB) Vel ΔSD**		10.3		14.9		22.3
$\boldsymbol{INR_{\mathrm{th}}}$ **(dB) SW ΔBias**		7.9		9.6		13.8
$\boldsymbol{INR_{\mathrm{th}}}$ **(dB) SW ΔSD**		2.4		4.5		-
$\boldsymbol{INR_{\mathrm{th}}}$ **(dB)**		**2.4**		**4.5**		**12.1**

3.3.5. Fraction of Range Gates Corrupted by Pulsed Interference

Pulsed interference does not contaminate all of the range gates within a dwell as CW interference does. The INR thresholds found earlier in this section do not change based on the interfering radar, but the number of range gates affected varies significantly. The PRTs of the two radars and the pulse length of the interfering radar are the main determinants of the fraction of range gates corrupted by interference, f_{c}. When the PRTs of the two interfering radars are not integer multiples, f_{c} is given by the equation from ITU-R M.1849 (2009) (Case II) with some slight modifications to match the notation in this paper:

$$f_{\mathrm{c}} = \frac{(\tau_{\mathrm{g}} + \tau_{\mathrm{i}})}{PRT_{\mathrm{i}}} \tag{3.3}$$

where PRT_{i} is the PRT of the interfering radar, τ_{g} is the range gate width in seconds (or sampling period), and τ_{i} is the pulse width of the interfering radar in seconds. The most used range gate spacing on the NEXRAD system is 250 m or $\tau_{\mathrm{s}} = 1.\bar{6}\mu$s. For an ASR-9 radar with a 1.05-μs pulse width, the fraction of corrupted range gates when $PRT_{\mathrm{i}} = 0.99$ ms is about 0.0027. The fraction of corrupted gates increases greatly for an ASR-11 radar with an 89-μs pulse width and a PRT_{i} of 1.17 ms ($f_{\mathrm{c}} = 0.077$) and is slightly less for an ASR-8 radar with a 0.6-μs pulse width and a PRT_{i} of 0.87 ms ($f_{\mathrm{c}} = 0.0026$). The parameters for the ASR radars were found in NTIA TR-13-490 (2012). When the PRTs are integer multiples, fewer range gates are affected but the range gates that are affected have multiple hits of pulsed interference instead of just a single hit.

In the cases other than the ASR-11, the fraction of corrupted gates is relatively small, but it is difficult to quantify the impact on forecasters and algorithms. The assumption for this study is that the corrupted gates are not meeting the derived requirements at these range gates, and that the effects could be significant if the interference occurs in the wrong place at the wrong time. A study that looked at the overall effects of pulsed interference on different weather cases would be a significant effort and is beyond the scope of this work.

3.4. Continuous Wave Interference

Continuous wave interference is on the other extreme from single-hit pulsed interference because all of the samples at a particular range gate are affected. We are using CW interference as a type of worst-case pulsed interference to show how the INR thresholds are reduced when more samples are contaminated. CW interference is also different from pulsed interference because it has a particular velocity, v_{CW}, that can influence the INR thresholds. Unlike the pulsed interference, only the ΔBias is examined for reflectivity, velocity, and spectrum width. Because the CW interference is a tone, the standard deviation of the combined weather and interference signals generally decreases as the INR increases. Hence, ΔBias is the driver of the INR thresholds for CW interference.

3.4.1. Reflectivity

The reflectivity ΔBias is displayed in Figure 8 for the same four cases that were utilized in the pulsed interference simulations. The curves indicate the same dependence of ΔBias on INR that we saw for pulsed interference. The main difference

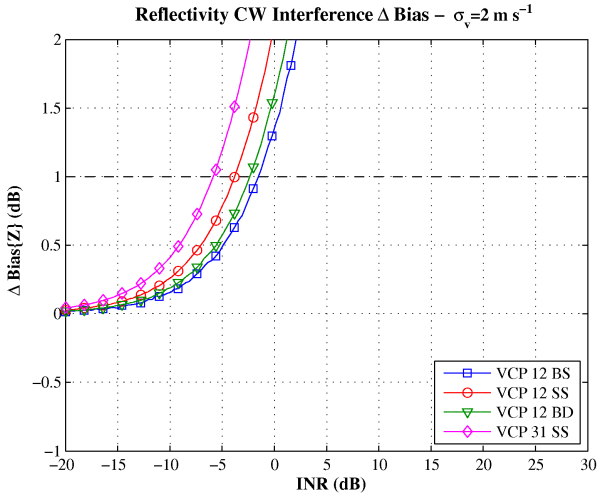

Figure 8: Reflectivity ΔBias as a function of INR for CW interference depicting the four cases from VCP 12 and 31. The 1-dB limit is denoted by the dashed horizontal line. Note the lower tolerance for CW interference as compared to the pulsed interference in Figure 5(a).

is that the INR thresholds are lower for CW interference than for pulsed interference. Another difference is that the default SNR thresholds have more effect on the INR thresholds than the number of samples. Notice that the lowest $INR_{\rm th}$ occurs for the VCP 31 SS case with a default SNR threshold of 0 dB. The next highest $INR_{\rm th}$ is the VCP 12 SS case with a default SNR threshold of 2 dB. The highest INR thresholds correspond to the two cases with a default SNR threshold of 3.5 dB, VCP 12 BD and VCP 12 BS. Between these two, the highest $INR_{\rm th}$ corresponds to the case with the fewest number of samples, VCP 12 BS. For the reflectivity estimator, the interference velocity, $v_{\rm CW}$, does not affect the results.

The INR thresholds for all four cases are shown in Table 5, along with results for the radial velocity and spectrum width estimators. These results are for a true spectrum width of 2 m s^{-1}; additional results for other spectrum widths and the 0.5 and 2-dB limits are presented in the full report.

3.4.2. Radial Velocity

The velocity ΔBias for the VCP 12 BD case is shown in Figure 9(a). This is different from the pulsed interference figure

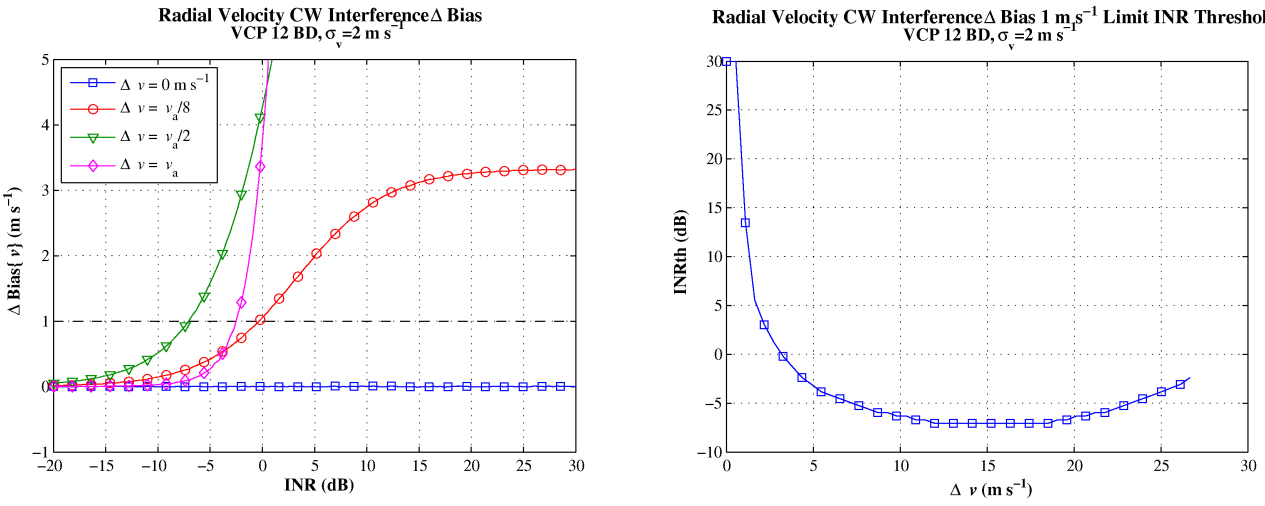

(a) (b)

Figure 9: Radial velocity (a)ΔBias as a function of INR for the VCP 12 batch Doppler case depicting various values of Δv and (b)INR thresholds as a function of Δv. The upward trend at high Δv values is a result of the relationship between the overlaid echoes at those particular signal-to-interference ratios in (b). The 1-m s^{-1} limit is presented as the dashed black line in (a).

because only one case (VCP 12 BD) is shown with four different Δv values. Δv is the absolute value of the difference between the interference velocity and the weather velocity. The ΔBias curves approach an asymptote equal to the Δv values at high INR. As mentioned previously, the interference velocity, v_{CW}, does have an effect on the INR thresholds, and this is reflected in the different INR thresholds for different Δv values. Because of this dependence, the effect on the INR thresholds will be further explored for a complete range of velocities.

Figure 9(b) illustrates the dependence of the INR_{th} on Δv from 0 m s^{-1} to v_{a}. One would anticipate that the 1-m s^{-1} limit would be met at increasingly lower INR values as the Δv term increases. However, larger Δv values do not result in the minimum INR value. Instead, an upward trend can be observed at large Δv values. This upward trend is due to the relationship between the strength of the weather and interference signals as well as the Δv parameter, and can be explored through the use of a phasor diagram. Because there are multiple interference thresholds for the same case, we need to determine a method to choose the overall INR_{th}. By picking the worst case value from Figure 9(b), we can ensure that the velocity meets the derived requirements for all possible values of Δv (unknown in practice). In this case, the INR thresholds are relatively flat around $v_{\mathrm{a}}/2$, so it seems reasonable to choose the worst case value.

Table 5 contains the worst case INR_{th} values for all three velocity cases. The values are very similar for all three cases and are lower than the reflectivity INR thresholds. This shows that the velocity estimator is more sensitive to CW interference than the reflectivity estimator.

3.4.3. Spectrum Width

The spectrum width ΔBias displayed in Figure 10(a) also shows a dependence on Δv similar to the velocity. The figure displays only one case (VCP 12 BD) for four Δv values. The dependence is more complicated because it increases with INR,

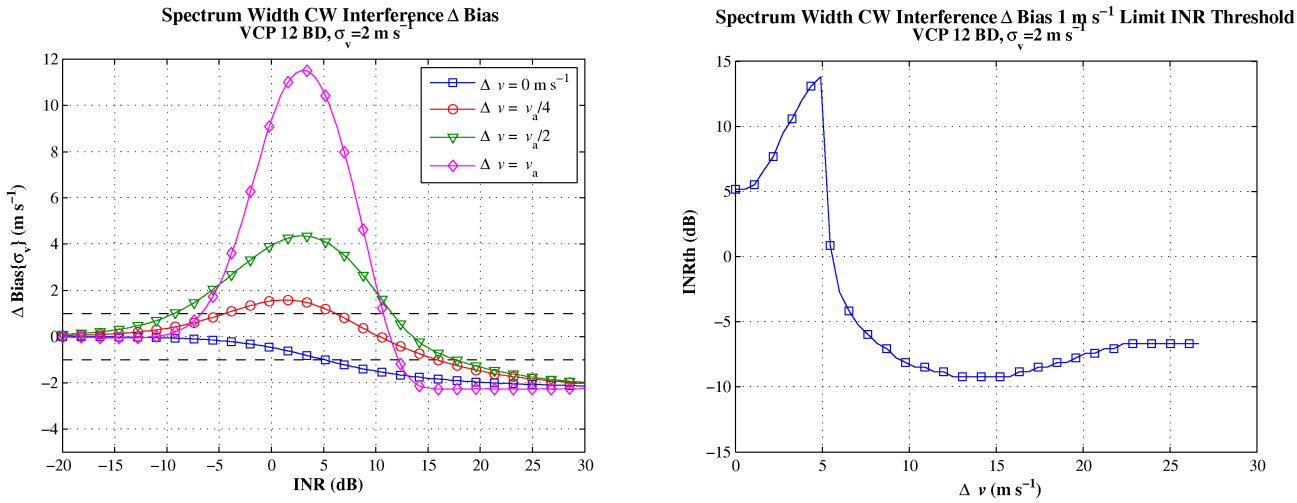

(a) (b)

Figure 10: Spectrum width (a)ΔBias as a function of INR for the VCP 12 batch Doppler case depicting various values of Δv and (b)INR thresholds as a function of Δv. As with the radial velocity ΔBias curves, a dependence on the Δv term is evident. The 1-m s^{-1} limit is depicted for both positive and negative values with the two dashed black lines in (a).

and then converges to a negative value at very high INR. Some of the curves have a peak because of the bimodal nature of the combined weather and interference spectrum. When the powers of the two signals are similar and the signals are separated in the spectrum, the spectrum width values can be large because the velocities are spread out between both signals. As the CW interference starts to dominate, the measured spectrum width approaches zero, which leads to the negative ΔBias at high INR. Note that the $\Delta v = v_{\mathrm{a}}$ curve crosses the other curves on both sides of the peak. This occurs because of increased use of the R_1/R_2 estimator and results in less sensitivity to interference at larger Δv. In addition, only three of the curves cross the positive 1-m s^{-1} limit, which results in some interesting behavior in Figure 10(b).

Figure 10(b) shows the dependence of the INR_{th} on Δv for the VCP 12 BD case. The sharp discontinuity in this figure is due to the fact that the ΔBias curves do not cross the positive 1-m s^{-1} limit at small Δv values, but do eventually cross the negative 1-m s^{-1} limit. At the Δv value where the ΔBias starts to cross the positive 1-m s^{-1}limit, the INR_{th} abruptly shifts resulting in the discontinuity. The INR_{th} increases slightly at larger Δv values. This is similar to the behavior of the velocity ΔBias except that the mechanism is different. As with the velocity, we use the worst case value for the INR_{th}. This ensures that the spectrum width meets the derived requirements under all conditions.

Table 5 captures the INR thresholds for spectrum width for all three cases. The spectrum width is the most sensitive to CW interference, and this is mainly due to the bimodal nature of the combined weather and interference signals.

3.4.4. Results Summary

Table 5 combines the results for all three meteorological variables into one table with the minimum $INR_{\rm th}$ for each case gathered in the bottom row. The spectrum width estimator is the driver in all three cases. These results show that the presence

Table 5: INR Thresholds - CW Interference - Summary - σ_v= 2 m s^{-1}

	VCP 12				VCP 31	
Scan	**BS**	**BD**	**SS**	**SD**	**SS**	**SD**
$\boldsymbol{INR_{\rm th}}$ **(dB) Ref ΔBias**	-1.5	-2.4	-3.8		-5.9	
$\boldsymbol{INR_{\rm th}}$ **(dB) Vel ΔBias**		-7.1		-6.7		-6.7
$\boldsymbol{INR_{\rm th}}$ **(dB) SW ΔBias**		-9.2		-9.2		-8.8
$\boldsymbol{INR_{\rm th}}$ **(dB)**		**-9.2**		**-9.2**		**-8.8**

of CW interference in all of the samples (as opposed to only one or a few for pulsed interference) greatly affects the INR thresholds. Pulsed interference at all samples would result in somewhat higher INR thresholds than CW interference since the interference signal would not be a tone.

4. Noise-Like Interference

Noise-like interference was not included in the simulations in the previous section because of a recent upgrade to the NEXRAD system. A new radial-by-radial noise estimator has been implemented that measures the noise power independently for each radial instead of using a single value for all of the radials in an elevation (Ivić et al., 2013). Noise-like interference increases the inherent system noise power. If the noise power estimate is not updated, the wrong noise power is used when estimating some of the meteorological variables. With the advent of the radial-by-radial noise estimator, the noise power is measured dynamically and more accurately, and the noise-like interference should not induce a bias in the estimation. The radial-by-radial noise estimator can remove the strobing effect that is often seen with noise-like interference, but the interference still degrades the meteorological-variable estimates. The main effect of noise-like interference will now be a decrease in the sensitivity of the radar where the interference is present. This loss in sensitivity is a serious issue since it can cause weaker weather signals to be censored (removed) from displays and algorithms.

As with the other types of interference, we look to the requirements to determine the $INR_{\rm th}$ for noise-like interference. The main sensitivity requirement states that "the RDA minimum detection capability in both the H and V channels shall (1) provide at least a 0 dB signal to noise ratio for a -4.5 dBZe target at 50 km." This requirement was changed before the dual polarization upgrade because of the expected loss of sensitivity when the transmit power was split between two polarizations. Overall, the current average baseline performance of the NEXRAD system provides a 0-dB SNR for a -9.5-dBZe target at 50 km. The ROC is planning on changing the requirement to "0 dB SNR for a -9.5 dBZe target at 50 km" to match the actual performance of the radars. If we base the $INR_{\rm th}$ on the current stated requirement and the baseline performance, then we need to find out how much the noise power can be increased by interference when the signal is 5 dB stronger [-4.5 dB - (-9.5 dB)]. This $INR_{\rm th}$ can be found using the following equation:

$$INR = 10\log_{10}\left(10^{\frac{R-B}{10}} - 1\right), \tag{4.1}$$

where R is the requirement in dBZe and B is the baseline performance of the system in dBZe. The $INR_{\rm th}$ in this case would be about 3.35 dB. This threshold should certainly be seen as an upper limit. An $INR_{\rm th}$ of 0 dB would lead to a doubling of the noise power which would cause a 3 dB loss of sensitivity. This is a significant loss in sensitivity and is one reason that the requirement is being updated. If we instead use the -9.5 dBZe requirement proposed by the ROC that matches the baseline performance, then no noise-like interference would be acceptable.

5. Looking Forward

The main purpose of this study is to look at the effects of interference on the NEXRAD system as it currently exists. For example, the radial-by-radial noise estimator changes the way that noise-like interference affects the system. This upgrade will soon be deployed across the NEXRAD network and will be turned on by default. Other upgrades will not be turned on by default, such as Coherency Based Thresholding (CBT). In this section, we will examine some of the possible upgrades to the NEXRAD radars and a possible future radar replacement. Of course, we cannot exactly foresee the future path of the NEXRAD network, but we can make some reasonable guesses about changes that could be relevant to the issue of interference.

In this section, we focus on three such areas: Pulsed Interference Filtering, Coherency Based Thresholding, and the Multi-function Phased Array Radar (MPAR). Each area is briefly introduced, and its effects on interference are discussed.

5.1. Pulsed Interference Filtering

There are certainly additional signal processing upgrades that could be made to the system to mitigate the effects of electromagnetic interference. One area that could be addressed with relatively simple filters is pulsed interference. Strong spikes in the Level-I (or time series) data can be detected relatively easily, but there are two main issues that can limit the effectiveness of pulsed interference filters. The first issue is determining what to replace the interference spike with if one is detected. There are concerns with interpolating across samples at a particular range gate if there are multiple signals present such as weather and clutter. Interpolating in range can also be problematic since the samples are not significantly correlated in range when the range gates are similar to the pulse length (250 m). Before a pulsed interference filter is implemented, the best way to interpolate the signal should be studied, and the effects of replacing an interference spike with interpolated data should be considered. The second issue that can limit the effectiveness of a pulsed interference filter is the difficulty of detecting weak interference spikes. If a filter is especially sensitive to spikes, it can filter some of the noise values and affect the measurement of noise in a radial. This can lead to estimation errors at low SNRs especially for the correlation coefficient which is very sensitive to noise. If a filter is not as sensitive to noise spikes, then weak interference spikes could still pass through the filter. These weak interference spikes could be large enough to bias the meteorological variable estimates without being apparent to the user. Pulsed interference filters should certainly be explored for use on NEXRAD radars, but will not solve all of the issues associated with pulsed interference.

5.2. Coherency Based Thresholding

As mentioned at the beginning of the section, Coherency Based Thresholding (CBT) is a future upgrade for the NEXRAD network, but will not be turned on by default. CBT is a technique that attempts to recover some of the signals that are lost because of the reduction in sensitivity due to the dual polarization upgrade. The transmitter power is split in half in order to transmit both horizontal and vertical polarizations which results in a 3 dB loss of sensitivity. Because of some additional losses in the hardware, the total sensitivity loss is somewhat larger than 3 dB. CBT looks at additional attributes of the weather signal to recover weaker, yet coherent signals and increase the data coverage; this technique cannot increase the inherent sensitivity of the radar, but can recover a significant number of weak weather signals that would otherwise be lost. CBT was not considered when running the simulations since it will not be on by default, but it could be used more in the future and could possibly be turned on for all radars. The main consequence for interference is that weather signals that are up to 3 dB below the current default SNR thresholds could be displayed. This could lead to across-the-board reductions in previously calculated INR thresholds. An additional study would be necessary to fully quantify the effects.

5.3. Multifunction Phased Array Radar

In the future, the NEXRAD network could be replaced by a network of multifunction phased array radars (MPAR). These MPARs would combine both weather and aircraft surveillance in a single system. The most likely antenna configurations for these radars are either a four-panel planar array or a cylindrical array. In both cases, it is likely that multiple frequencies would be needed to mitigate interference between two antenna faces or two segments of a cylindrical array. It may also be necessary to use multiple frequencies in order to satisfy the requirements of multiple surveillance functions.

A network of MPARs could save a significant amount of money in the long term because of reduced maintenance and a reduction in the total number of radar systems. The radar systems that might be replaced by MPAR (or a smaller, scalable terminal MPAR) include the C-band Terminal Doppler Weather Radar (TDWR), the S-band ASR-9 and ASR-11, and the L-band air route surveillance (ARSR) radars. Since the current plan is for both the MPAR and terminal MPAR to be S band, this could possibly free up some spectrum in the other bands. But, the possible need for more frequencies compared to current radar systems could put even more demands on S band. The consequences of a future MPAR network should be considered when making decisions about the electromagnetic spectrum.

6. Conclusions

This study quantifies the effects of pulsed, continuous wave, and noise-like interference on the estimation of spectral moments and dual-polarimetric variables for NEXRAD radars. Our approach was to define the INR thresholds based on the NEXRAD technical requirements. Because there are no requirements that specifically address interference, we derived a set of requirements that extend the original requirements to interference. These new requirements set limits on the amount of additional bias and standard deviation that can be induced by interference. The limits were set to 1 dB for reflectivity and 1 m s^{-1} for radial velocity and spectrum width. These limits are directly based on the NEXRAD standard deviation requirements and have been used in previous interference reports. Because of the performance of polarimetric-variable estimators at low SNRs, only the spectral moments were used to determine INR thresholds.

Simulations were developed to quantify the effects of both pulsed and continuous wave interference on the meteorological-

variable estimators. Several different sets of simulations were examined to find the best way to quantify the effects of interference. Data were simulated using parameters from two sweeps from VCP 12 and one sweep from VCP 31. These VCPs were identified as the most sensitive to interference. The simulations added interference signals to simulated weather signals, and the effects could be measured because the parameters of the weather signals are known. The interference signals were based on interference models that were described mathematically in the text. After the simulations were run, statistics were computed from the simulated time series so that ΔBias and ΔSD values could be computed. The ΔBias and ΔSD values were then used to determine INR thresholds based on the derived requirements. For continuous wave interference, the effects of different interference frequencies were explored, and the INR thresholds were based on the worst-case performance. The INR thresholds were collected in tables for each of the spectral moments, and summary tables were provided to capture the minimum INR_{th} for each case. The most stringent INR thresholds are 2.4 dB for pulsed interference and -9.2 dB for continuous wave interference, with other values provided for different sweeps and elevation angles. The fraction of range gates corrupted by pulsed interference was also investigated based on a formula from a previous technical report. Specific values were computed for the ASR-8, ASR-9, and ASR-11 radars.

Noise-like interference was not included in the simulations because the main effect of this type of interference is a loss of sensitivity. The recently implemented radial-by-radial noise estimation technique eliminates the biases induced in some of the meteorological-variable estimators. Sensitivity loss is now considered to be the most significant consequence of noise-like interference. Based on the current baseline performance of the NEXRAD system, we showed that an INR_{th} of about 3.35 dB was needed to meet the current requirements. This is a conservative estimate because the effects of noise-like interference on the sensitivity can be seen at much lower INR thresholds. If the ROC changes the sensitivity requirement to match the current baseline performance, no noise-like interference could be tolerated.

The impacts of some possible future upgrades were also considered. The NEXRAD system is always changing and new algorithms or a multifunction phased array replacement could greatly affect the frequency requirements the system. These future demands should be considered when determining the siting and frequency allocation for weather and other surveillance radars.

Acknowledgement

We would like to thank Bob Denny for providing additional information including documentation and teleconferences that supported our research. Both John Carroll and Frank Sanders participated in a teleconference to answer questions and provide technical information. We also appreciate the feedback from Russ Cook, Dave Zittel, Glenn Secrest, Lynn Allmon, Rich Ice and Dave Franc that helped guide the direction of the study. Sebastian Torres reviewed multiple versions of the document, which led to significant improvements in the final product.

This paper was prepared by Brad Isom and Christopher Curtis with funding provided by NOAA/Office of Oceanic and Atmospheric Research under NOAA-University of Oklahoma Cooperative Agreement #NA11OAR4320072, U.S. Department of Commerce. The statements, findings, conclusions, and recommendations are those of the authors and do not necessarily reflect the views of NOAA or the U.S. Department of Commerce.

References

C. D. Curtis and B. M. Isom, "The effects of interference on NEXRAD: A requirements-based approach," National Severe Storms Laboratory, Norman, OK, Tech. Rep., 2014.

M. Fang, R. J. Doviak, and V. Melnikov, "Spectrum width measured by WSR-88D: Error sources and statistics of various weather phenomena," *J. Atmos. Oceanic Technol.*, vol. 21, pp. 888–904, 2004.

G. Galati and G. Pavan, "Computer simulation of weather radar signals," *Simulation Practice and Theory*, vol. 3, pp. 17–44, 1995.

ITU-R Recommendation M.1464, "Characteristics of and protection criteria for radionavigation and meteorological radars operating in the frequency band 2700-2900 MHz," International Telecommunication Union, Radiocommunication Sector, Tech. Rep., 1998.

ITU-R Recommendation M.1849, "Technical and operational aspects of ground-based meteorological radars," International Telecommunication Union, Radiocommunication Sector, Tech. Rep., 2009.

I. Ivić, C. Curtis, and S. Torres, "Radial-based noise power estimation for weather radars," *J. Atmos. Oceanic Technol.*, vol. 30, pp. 2737–2753, 2013.

NCAR, "Improving NEXRAD data: Data quality algorithm progress (FY2009 Annual Report)," National Center for Atmospheric Research, Boulder, CO, Tech. Rep., 2009.

ROC, "WSR-88D system specification 281000H," WSR-88D Radar Operations Center, Norman, OK, Tech. Rep., 2008.

F. H. Sanders, R. Sole, B. Bedford, D. Franc, and T. Pawlowitz, "Effects of interference on radar receivers," U.S. Dept. of Commerce, Tech. Rep. NTIA Technical Report TR-06-444, 2006.

F. H. Sanders, R. L. Sole, J. E. Carrol, G. S. Secrest, and T. L. Allmon, “Analysis and resolution of RF interference to radars operating in the band 2700-2900 MHz from broadband communication transmitters,” U.S. Dept. of Commerce, Tech. Rep. NTIA Technical Report TR-13-490, 2012.

D. S. Zrnić, “Simulation of weatherlike Doppler spectra and signals,” *J. Appl. Meteor.*, vol. 14, pp. 619–620, 1975.